Geochimica et Cosmochimica Acta, Vol. 69, No. 17, pp. 4211–4225, 2005

0016-7037/05 $30.00 + .00

doi:10.1016/j.gca.2005.04.013

Immobilization of Ni by Al-modified montmorillonite: A novel uptake mechanism

Maarten Nachtegaal,[1,*] André M. Scheidegger,[2,3] Rainer Dähn,[2] Daniel Chateigner,[4] and Gerhard Furrer[1]

[1]Institute of Terrestrial Ecology, ETH Zürich, CH-8952, Schlieren, Switzerland
[2]Laboratory for Waste Management, Paul Scherrer Institute, CH-5232 Villigen, Switzerland
[3]MicroXAS beamline, Swiss Light Source (SLS), Paul Scherrer Institute, CH-5232, Villigen, Switzerland
[4]Laboratoire de Cristallographie et Sciences des Matériaux (CRISMAT), Ecole Nationale Supérieure d'Ingénieurs de Caen (ENSICAEN), 14050 Caen, France

(*Received September* 7, 2004; *accepted in revised form March* 31, 2005)

Abstract—The sorption capacity of montmorillonite clay minerals for small cations, such as Ni^{2+}, can be greatly enhanced by modifying the clay mineral with Al(III). In this study, the mechanisms of Ni uptake by Al-modified montmorillonite were studied using extended x-ray absorption fine structure (EXAFS) spectroscopy of powders and polarized EXAFS spectroscopy of self-supporting clay films to delineate the binding structure of Ni formed as a function of the reaction conditions. Analysis of powder EXAFS spectra of wet pastes, collected from Ni-treated Al-modified montmorillonites reacted at pH 5–8, 25°C or 80°C (to accelerate the reaction process), and reaction times ranging from 1 month to 9 yrs, showed that Ni was surrounded on average by 6 O atoms at a distance of 2.05 Å and 6 Al atoms at 3.01 Å, suggesting the incorporation of Ni into a gibbsite-like structure. Only at pH 8, Ni-containing precipitates were congruently formed. Polarized EXAFS spectroscopy of self-supporting Ni-reacted Al-modified montmorillonite clay films showed a pronounced angular dependency of the spectra of the Ni-doped gibbsite, indicating that the orientation of this Ni-doped gibbsite coincided with the layering of the montmorillonite. Data analysis suggested that Ni is included slightly above and below the vacant octahedral sites of the postulated interstitial gibbsite monolayer. This newly identified mechanism of metal uptake by Al-modified montmorillonite provides a large metal sorption capacity and, because the metal is included in a monolayer gibbsite or gibbsite "islands" formed in the interstitial space of the clay mineral, it potentially leads to a permanent sequestration of the metal from the environment. *Copyright © 2005 Elsevier Ltd*

1. INTRODUCTION

Smectites are 2:1 clay minerals, where two tetrahedral sheets are bonded to one octahedral sheet (Güven, 1988). Owing to their high sorption capacity, smectites have been proposed as possible sinks for heavy metals in *in situ* remediation projects of large contaminated areas, liners in waste deposits, and backfill material in nuclear waste repositories. On montmorillonite, a dioctahedral smectite (dioctahedral meaning that two out of three octahedral sites are occupied), the tetrahedral positions are filled with Si, whereas the octahedral positions are filled by Al. Like most clay minerals, montmorillonite possesses both planar and edge sites capable of sorbing trace metal ions such as Ni^{2+}. A permanent negative charge exists on planar sites owing to isomorphic substitutions (partial replacement of Al^{3+} by Fe^{2+} and Mg^{2+}) in the octahedral layers (Güven, 1988; Sparks, 2003). Interaction with planar surfaces mainly occurs by electrostatic interactions, whereby the metals retain their primary hydration sphere upon interaction with the montmorillonite. Edge sites are formed by broken Al-OH and Si-OH bonds and protonate or deprotonate depending on pH (McBride, 1994). At edge sites, Ni can be held electrostatically or specifically by forming a chemical bond with the hydroxyl groups.

Extended x-ray absorption fine structure (EXAFS) spectroscopic studies, investigating the uptake mechanisms of Ni on smectite clay minerals, have shown that Ni uptake by smectite clay minerals depends on the ionic strength, pH, metal concentration, and reaction time (Scheidegger et al., 1998; Elzinga and Sparks, 2001; Dähn et al., 2002, 2003).

At low pH (<5.0) and Ni concentrations <6 mM, no backscattering contribution from second neighboring Ni, Al, or Si atoms was observed in the EXAFS spectra. Consequently, it can be concluded that Ni is mainly electrostatically held, with water molecules bridging Ni to the basal planes of the clay mineral particles (Dähn, personal communication).

At higher pH (>5.0), and at low Ni concentrations (0.020 mM), Ni was found bound to two Al atoms at ~3.0 Å, two Si atoms at ~3.12 Å, and four Si atoms at ~3.26 Å, indicating chemisorption, or alternatively specific sorption, of Ni at the edge sites of montmorillonite (Dähn et al., 2003).

At higher pH (>6.0) and higher initial Ni concentrations (>0.1 mM), newly formed Ni containing mineral phases were observed. Using powder EXAFS, Scheidegger et al. (1998) observed newly formed Ni phases when Ni (3.0 mM) was reacted with montmorillonite at pH 7.5. Further studies (Elzinga and Sparks, 2001) showed that the Ni precipitate forms at pH values as low as 6.25. The rate of formation for these new Ni phases thereby depends on the pH and increases with increasing pH. In a polarized EXAFS (P-EXAFS) study, Dähn et al. (2002) showed that the precipitates formed in the Ni-montmorillonite system under these reaction conditions (pH 8, $[Ni]_{initial}$ = 0.66 mM) resemble, in fact, a Ni-phyllosilicate phase, rather than a mixed Ni-Al layered double hydroxide (LDH) precipitate, as suggested by the earlier bulk EXAFS studies (Scheidegger et al., 1998). Dähn et al. (2002) were able to demonstrate this thanks to the use of P-EXAFS. The use of

* Author to whom correspondence should be addressed (maarten.nachtegaal@psi.ch).

P-EXAFS spectroscopy allows overcoming the strong overlap of scattering contributions of cations (Ni and Al) at $3.0 \leq R \leq 3.1$ Å in the octahedral sheet and cations (Si) at $3.15 \leq R \leq 3.23$ Å in the tetrahedral sheets.

The scientific interest in the sorption mechanisms of Ni onto clay minerals arises from the following reasons: (1) Ni belongs to the suite of toxic metals (Ni, Cu, Zn, Cd, Pb, and Hg) that are subject to concentration limits in drinking water, and (2) large amounts of ^{59}Ni and ^{63}Ni, with half-lives of 75,000 and 125 yrs, respectively, occur as fission products in nuclear waste (Hummel and Curti, 2003).

The sorption properties of montmorillonite clays for small cations such as Ni^{2+}, Cu^{2+}, and Zn^{2+} can be strongly improved when the clay mineral is modified with monomeric Al(III) species or with the Al_{13} Keggin ($AlO_4Al_{12}(OH)_{24}\cdot(H_2O)_{12}{}^{7+}$(aq)) species (Harsh and Doner, 1984; Furrer et al., 1994). In a batch metal uptake study, Ni^{2+}, Cu^{2+}, and Zn^{2+} were found to specifically sorb on Al-montmorillonite compounds (Lothenbach et al., 1997). This finding was based on the fact that Ni, Cu, and Zn remained immobilized in the solid phase after a large excess of barium cations was applied to the metal-reacted Al-modified montmorillonite. For comparison, most heavy metals were remobilized when untreated montmorillonite was subjected to a large excess of barium cations (Lothenbach et al., 1997).

The above findings were solely based on macroscopic investigations. Therefore a molecular-level understanding on the uptake mechanisms of metal ions onto Al-modified montmorillonite is still needed, to obtain specific information on the Ni sorption mechanism and stability of the sorption complex formed.

In the present study, the molecular-scale uptake mechanism of Ni onto Al-modified montmorillonite was investigated using P-EXAFS. The uptake process was investigated for a variety of experimental conditions (pH (5–8), time (1 month–9 yrs), and temperature (25°C–80°C)) to elucidate the effect of reaction conditions on the fate of Ni in Al-modified montmorillonite suspensions. Applying P-EXAFS to Ni-reacted Al-modified montmorillonite clay films has the advantage over powder EXAFS in that the orientation of the Ni bond pairs with respect to the layering of the clay minerals can be probed (Manceau et al., 1998).

2. MATERIALS AND METHODS

2.1. Materials

Na-Montmorillonite (Mont) SWy-1 (Crook County, Wyoming) was purchased from the Source Clay Minerals Repository of the Clay Mineral Society. X-ray diffraction of the "as-received" montmorillonite indicated the presence of minor quantities of quartz. The stoichiometry of the SWy-1 clay (determined with XRF) is $(Si_{8.0}Al_0)^{IV}\cdot(Al_{3.06}Fe_{0.4}Mg_{0.51})^{VI}O_{20}(OH)_4(Ca_{0.15}Na_{0.06}K_{0.01})$ and its total iron content is ~4.5%. The montmorillonite was thoroughly washed with 1 M $NaClO_4$ to remove all soluble salts and to change the clay into the homoionic form. The ≤0.5 μm fraction was separated by successive washing with deionized water, combined with centrifugation (Baeyens and Bradburry, 1995). Soluble hydroxy-aluminum compounds were removed by acidic treatment (pH 3.5 for 1 h) of the clay suspension. The pH was subsequently readjusted to 7.

Al-modified montmorillonite (Al-mont) was prepared by adding Al(III) from a 0.1 M $AlCl_3$ stock solution to the montmorillonite stock suspension, so that a ratio of 2 mM Al(III) per gram of montmorillonite was reached (Lothenbach et al., 1997). Before the Ni uptake experiments, the Al-modified clay suspension was slowly titrated to pH 5 using a computer-controlled pH stat (Metrohm 736).

Al_{13} was prepared, following the procedure outlined in Furrer et al.(1993), by adding 1000 mL of 1 M NaOH stepwise to 1500 mL 0.25 M $AlCl_3$ at 80°C in a temperature-controlled reaction vessel and under continuous stirring. The dosing was conducted using a pH stat (Metrohm 736). The final neutralization ratio r_{OH} (which is defined as $[OH]_{tot}/[Al(III)]_{tot}$) was 2.4. Following preparation of Al_{13}, the solution was analysed by ^{27}Al NMR spectroscopy to verify the purity of the Al_{13} solution.

2.2. Sample Preparation for Powder and Polarized EXAFS

2.2.1. *Preparation of Ni-reacted Al-modified montmorillonite samples*

The interaction of Ni with Al-modified montmorillonite (Al-mont) was studied using a batch-type setup. Ni uptake was studied as a function of final solution pH (5–8), reaction time, and temperature. Al-modified montmorillonite suspensions with a solid/solution ratio 2g L^{-1} and with a background electrolyte of 0.1 M $NaClO_4$ were prepared from the stock solution (section 2.1). Nickel, from an acidified 0.1 M $NiCl_2$ stock solution, was added in 0.5 mL aliquots to the Al-montmorillonite suspensions to achieve an initial Ni concentration of 0.1 mM. Except for the pH 8 solution, all solutions were undersaturated with respect to homogeneous precipitation of $Ni(OH)_2$ (Hummel and Curti, 2003). Samples were reacted with Ni for 1 month in a batch setup, with a pH stat to control the pH. To speed up the reaction process, some samples were prepared in an 80°C warm water vessel and subsequently stored at 80°C. The pH was adjusted every other day. In this study we also investigated samples that were reacted with Ni for 9 yrs. These samples were taken from a study by Lothenbach et al. (1997) and were prepared under similar conditions and stored in the dark at room temperature.

All Ni-reacted suspensions were vacuum filtrated under a continuous flow of Ar gas. The supernatant solution was analyzed for Ni by flame AAS. The sorbed concentrations of Ni were calculated from the difference between initial and final concentrations in solution. The wet pastes were loaded into polyethylene sample holders which were sealed with Kapton polyamide tape.

Highly oriented clay films for P-EXAFS analysis were prepared from a sample that reacted with Ni for 1 month at pH 5 at 80°C (Al-mont–pH5–OV) and from a sample that reacted with Ni for 9 yrs at pH 7 at room temperature (Al-mont–pH7–9yrs). These two Ni-reacted suspensions were slowly vacuum filtered under a continuous flow of Ar, using a Millipore filter with 0.4 μm pore size. The supernatants were analyzed for Ni using flame AAS. Excess solution in the wet film was removed by washing with a few milliliters of deionized water before drying. The film was air dried for 48 h at room temperature, after which the dried clay film was cut into slices and stacked on a sample holder to get sufficient thickness for measurements in fluorescence detection mode (Dähn et al., 2002). A summary of the sample notation used in this manuscript, the experimental conditions (pH, reaction time, and temperature), as well as the amount of Ni taken up by Al-montmorillonite (μmol/g), is shown in Table 1.

2.2.2. *Ni reference spectra*

EXAFS spectra of Ni montmorillonite sorption samples, encompassing different Ni sorption modes, were obtained from Dähn et al. (2002, 2003). Ni-reacted Al_{13} was prepared by adding Ni from an acidified 0.1 M $NiCl_2$ stock solution to the Al_{13} stock solution, in such a way that a Ni to Al_{13} ratio of 0.1 mM Ni to 0.3 mM Al_{13} was achieved. This solution was slowly titrated to pH 6 and subsequently filtrated.

2.3. Quantitative Texture Analysis of Clay Films

Quantitative texture analysis of the two Ni-reacted Al-modified montmorillonite clay films was carried out by X-ray diffraction experiments using a Huber texture goniometer in reflection mode and monochromatized Cu Kα radiation collimated to a 0.5 × 0.5 mm parallel beam. One slice of each self-supporting film was mounted on a single-crystal silicon wafer to avoid background interference in the measure-

Table 1. Experimental conditions for Ni uptake onto montmorillonite and Al-modified montmorillonite.

Sample notation	Sorbent	pH initial	pH final	Ionic strength	Solid:solution ($g.L^{-1}$)	[Ni] (mM)	Time and Temperature	Γ (μmol/g)
Reference Spectra								
Mont-pH5	Montmorillonite	5.0	5.0	0.005 M $Ca(NO_3)_2$	7.8	6.0	90 days-RT	144.3
Mont-pH7	Montmorillonite	7.0	7.0	0.3 M Na ClO_4	2.2	0.019	14 days-RT	4.0
Mont-pH8	Montmorillonite	8.0	8.0	0.2 M $Ca(NO_3)_2$	7.9	0.660	90 days-RT	62.8
Al_{13}	$AlO_4Al_{12}(OH)_{24}(H_2O)_{12}^{7+}$	6.0	5.7	0.1 M $NaClO_4$	0.3 mML^{-1}	0.1	9 years-RT	50.0
Polarized EXAFS								
Al-mont–pH5–OV	Aluminum-modified montmorillonite	5.0	5.0	0.1 M $NaClO_4$	2.0	0.1	1 month-OV	19.6
Al-mont–pH7–9yr	Aluminum-modified montmorillonite	7.0	6.7	0.1 M $NaClO_4$	2.0	0.1	9 years-RT	49.5
Bulk EXAFS								
Al-mont–pH6–RT	Aluminum-modified montmorillonite	6.0	6.0	0.1 M $NaClO_4$	2.0	0.1	1 month-RT	30.0
Al-mont–pH6–OV	Aluminum-modified montmorillonite	6.0	6.0	0.1 M $NaClO_4$	2.0	0.1	1 month-OV	44.3
Al-mont–pH6–9yr	Aluminum-modified montmorillonite	6.0	5.0	0.1 M $NaClO_4$	2.0	0.1	9 years-RT	28.1
Al-mont–pH8–OV	Aluminum-modified montmorillonite	8.0	8.0	0.1 M $NaClO_4$	2.0	0.3	1 month-OV	49.3

ments. The complete film texture can be obtained by measuring the inclination of {001} crystallographic planes off the film surface. Because the textures of self-supporting clay films are axially symmetrically around the film plane normal, only a tilt angle (ρ) scan is necessary to obtain the full orientation information (Manceau et al., 1998). The diffracted intensity is proportional to the number of montmorillonite planes satisfying the Bragg conditions of these reflections (Dähn et al., 2003).

The (004) pole figures of a single slice of each film were measured by scanning the tilt angle ρ between 0° and 85°, with angle increments of 5° and an integration time of 2 h for each tilt angle position. The densities of the orientation distribution were calculated from the diffracted intensities integrated over all ρ angles by means of direct normalization and taking a density of zero at $\rho > 80°$ (for an extensive description of the procedure employed, see Manceau et al., 1998). Distribution densities are expressed as a multiple of a random distribution (mrd) (Bunge and Esling, 1982) and are equal to 1 for a randomly oriented sample.

2.4. EXAFS Data Collection and Reduction

Ni K-edge XAFS spectra were collected at the Dutch Belgium beamline (DUBBLE, BM26) and the Swiss Norwegian beamline (SNBL, BM1) at the European Synchrotron Radiation Facility (ESRF), Grenoble, France. Spectra of wet pastes or highly oriented clay films were recorded at room temperature using a Si(111) monochromator. The monochromator was calibrated by assigning the first inflection point of the K absorption-edge spectrum of a Ni metal foil to 8333 eV. The measurements were carried out in fluorescence mode using either a 9-element Ge solid-state detector (BM26) or an Ar-filled Stern-Head type (Lytle) detector, equipped with a 6 μm Co filter and Soller slits (BM1). Several scans were averaged to improve the signal-to-noise ratio.

P-EXAFS spectra for the Al-mont–pH5–OV and the Al-mont–pH7–RT clay films were recorded with the electric field vector (ε) at $\alpha = 10°, 35°, 55°$, and 80° with respect to the film plane. By varying the angle between the electric field vector and the layer plane of a self-supporting clay film, P-EXAFS probes the local structure of layered minerals between two different directional limits, parallel ($\alpha = 90°$) and perpendicular ($\alpha = 0°$) to the (001) plane. From the analysis of the amplitude of the P-EXAFS of clay films, one measures an apparent number of neighbors ($NN_{j,\alpha}^{exafs}$), that are seen at angle α. This number of neighbors is modified by the spread of clay particles in the film plane (Manceau and Schlegel, 2001):

$$\frac{NN_{j,a}^{exafs}}{NN_j^{cryst}} = 1 - \frac{\left(3\cos^2\beta_j^{cryst} - 1\right)\cdot\left(3\cos^2\alpha - 2\right)}{2}\cdot I_{ord} \qquad (1)$$

where α is the angle between the electric field vector (ε) and the layer plane, β_j^{cryst} is the angle between the film normal and the vector R_{ij} (connecting the x-ray absorbing atom i to the backscattering atom j), and NN_j^{cryst} is the crystallographic number of atoms in the j shell. I_{ord} is the function that accounts for the particle disorder; its value is unity for perfectly ordered films and zero for an isotropic sample (Manceau and Schlegel, 2001). I_{ord} is defined as:

$$I_{ord} = \frac{\int_0^{\pi/2}\left(3\cos^2\alpha - 1\right)\exp\left(-\alpha^2 1n(2)/\Omega^2\right)\sin\alpha\cdot d\alpha}{2\int_0^{\pi/2}\exp\left(-\alpha^2 1n(2)/\Omega^2\right)\sin\alpha\cdot d\alpha} \qquad (2)$$

with Ω representing the half width of half maximum of the profile shape function used to model the distribution of the c* axis around the film normal. In this study I_{ord} was used to correct the bond angle (β) between the Ni-Al bond direction and the layering of the montmorillonite.

EXAFS data analysis was carried out using the WinXAS 3.1 software package (Ressler, 1998). The energy scale was converted to photoelectron wave vector units ($Å^{-1}$) by assigning the origin E_0 to the first inflection point of the absorption edge. Radial structure functions (RSFs) were obtained by Fourier transforming the k^3-weighted $\chi(k)$ functions (k is the photoelectron wavenumber) between 2.0 and 10.5 $Å^{-1}$ using a Bessel window function with a smoothing parameter of 4. Amplitude and phase shift functions were calculated with FEFF 8.0 (Ankudinov et al., 1998) using the structures of β -$Ni(OH)_2$, gibbsite and hydrotalcite as model compounds (Greaves and Thomas, 1986; Saalfeld and Wedde, 1974; Bellotto et al., 1996). Fits were performed in R space over the range of 1.0 to 3.7 Å. The amplitude reduction factor (S_0^2) was determined at 0.85 from the experimental β -$Ni(OH)_2$ XAFS spectrum. The deviation between the fitted and the experimental spectra (%Res) is given by:

$$\%\mathrm{Res} = \frac{\sum_{i=1}^{N}\left|y_{\exp}(i) - y_{theo}(i)\right|}{\sum_{i=1}^{N} y_{\exp}(i)}\cdot 100 \qquad (3)$$

where N is the number of points in the fit window, and y_{exp} and y_{theo} are the experimental and theoretical RSF values. The precision on the EXAFS distances (R) was previously estimated to be ±0.02 Å for $R_{Ni\text{-}O}$, ±0.03 Å for $R_{Ni\text{-}Al}$, and ±0.5 for the number of neighbors (NN) (Scheidegger et al., 1998; Schlegel et al., 2001a). The experimental uncertainty on α in the P-EXAFS measurements is ±1°.

Using the reference spectra and the ALS 10.3.2 in-house software utilities, a linear fitting approach was used to fit samples that are composed of different Ni species. Linear combinations of the references were optimized to fit the k^3-weighted $\chi(k)$ EXAFS spectra with only the fractions of each reference spectrum as adjustable parameter. Fits were optimized by minimizing the normalized sum-square (NSS =

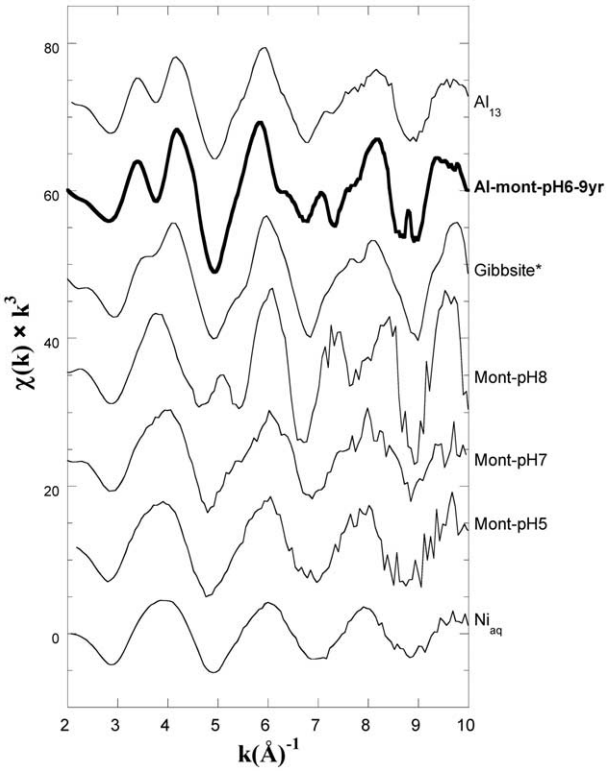

Fig. 1. k^3-weighted Ni K-edge EXAFS spectra of aqueous Ni, Ni-reacted montmorillonite at pH 5, 7, and 8 respectively, Ni-reacted gibbsite (* = Ni-reacted high surface area gibbsite (HS-Gb 30d, Yamaguci et al., 2002), Ni-reacted Al-modified montmorillonite, and Ni-reacted Al_{13}.

$\Sigma\,[k^3\chi(k)_{exp} - k^3\chi(k)_{reconstr.}] / \Sigma\,[k^3\chi(k)_{exp}]$) (Manceau et al., 2002). The accuracy of this fitting approach depends on the data quality, range of fitting, and how well the standards represent the unknown sample.

3. RESULTS

3.1. Powder EXAFS of Ni-Reacted Al-Modified Montmorillonite

Figure 1 shows in bold the k^3-weighted $\chi(k)$ EXAFS spectrum of the Al-modified montmorillonite suspension that has been allowed to react with a Ni solution at room temperature for 9 yrs (Al-mont–pH6–9yr). This spectrum displays a multifrequency wave shape, indicating the presence of more than one ordered neighboring shell around Ni. Furthermore the spectrum is characterized by a distinct splitting of the first oscillation at 3–4 Å and a small distinct peak at 7 Å.

Insight into the crystallochemical environment of sorbed Ni can be obtained by "fingerprinting" the spectrum of the Al-mont–pH6–9yr sample against the spectra of Ni with known sorption configurations. This is shown in Figure 1, where the Al-mont–pH6–9yr spectrum is compared to spectra of Ni sorbed onto the individual sorbents, i.e., montmorillonite, gibbsite, or titrated Al_{13}. The spectrum of montmorillonite reacted with Ni at pH 5 (Mont-pH5) is characteristic of Ni sorbed to montmorillonite as an outer-sphere complex (Dähn, personal communication). The spectrum is characterized by a monotonically decreasing sinus function, similarly as for the aqueous Ni spectrum, which is caused by a single coordinating oxygen shell. The spectrum of the pH 7 sorption sample (Mont-pH7) is characteristic of Ni bound to montmorillonite as an inner-sphere sorption complex (Dähn et al., 2003). The Mont-pH8 spectrum is characteristic of Ni incorporated into a neoformed surface-induced phyllosilicate precipitate (Dähn et al., 2002). Fingerprinting of the spectra of the Ni-reacted montmorillonite samples against the spectrum of the Ni-treated Al-modified montmorillonite (Al-mont–pH6–9yr) shows that none of the Ni-reacted montmorillonite reference spectra share similarities with the Al-mont–pH6–9yr spectrum.

The Ni-sorbed gibbsite spectrum was obtained from Dr. Scheinost (Yamaguchi et al., 2002) and is representative of Ni sorbed as an inner-sphere sorption complex at the gibbsite surface. This spectrum shares some similarities with the Al-mont–pH6–9yr sample, in that the first oscillation is split to some extent. The only reference spectrum, however, that shares the same distinct splitting of the first oscillation in the $k^3\chi(k)$ spectrum as the Al-mont–pH6–9yr sample is the spectrum of the Ni-reacted Al_{13}. Al_{13} is the ε-Keggin polyoxocation ($AlO_4Al_{12}(OH)_{24}(H_2O)_{12}^{7+}$). This aluminum phase is frequently formed in acidic environments (Furrer et al., 2002) and is used here as a proxy for amorphous Al phases or the reactive functional groups of Al mineral phases. The Ni-reacted Al_{13} reference was produced by slowly titrating an Al_{13} stock solution mixed with Ni (we could arbitrarily have taken a monomeric Al (III) solution) to pH 6, thus forming either gibbsite or an amorphous aluminum oxide, with Ni fully included in the aluminum structure. Consequently, the Ni uptake mode in the Al-modified montmorillonite suspensions resembles that of Ni sorbed to or included into an Al mineral, rather than to montmorillonite.

An increased reaction temperature (80°C) was used to speed up the aging process, and to bridge the time gap between the 9-year-old samples and more recently prepared suspensions (Fig. 2). All three spectra share common characteristic features in the spectra (e.g., splitting of the first oscillation), suggesting a similar uptake mode of Ni in the Al-modified montmorillonite samples. The intensity of the features in the spectra increase going from the $k^3\chi(k)$ spectrum of the suspension reacted for 1 month at room temperature (Al-mont–pH6–RT) (Fig. 2a) to the suspension reacted for 1 month at 80°C (Al-mont–pH6–OV) to the spectrum of the suspension reacted for 9 yrs at room temperature (Al-mont–pH6–9yrs). This indicates that the sorption kinetics were increased and the aging process was enhanced with an increased reaction temperature. It also suggests that the intrinsic Ni uptake mechanism remained unaltered by the increased reaction temperature.

The corresponding Fourier transforms are given in Figure 2b. Three major peaks, at $R + \Delta R$ of 1.6 Å, 2.5 Å, and 3.2 Å (labeled A, B, and C) could be distinguished in the RSFs. These peaks point to the presence of several neighboring atomic shells in the vicinity of sorbed Ni. The first major RSF peak (A) results from backscattering contributions from the nearest ligands and was best fitted with O atoms. Ni-O structural parameters derived from a multiple shell fit in R space are given in Table 2. In all three Al-modified montmorillonite samples, Ni is surrounded by ~6 oxygen atoms at a radial distance of 2.02–2.04 Å, suggesting octahedral coordination.

The second RSF peak (B) results from backscattering con-

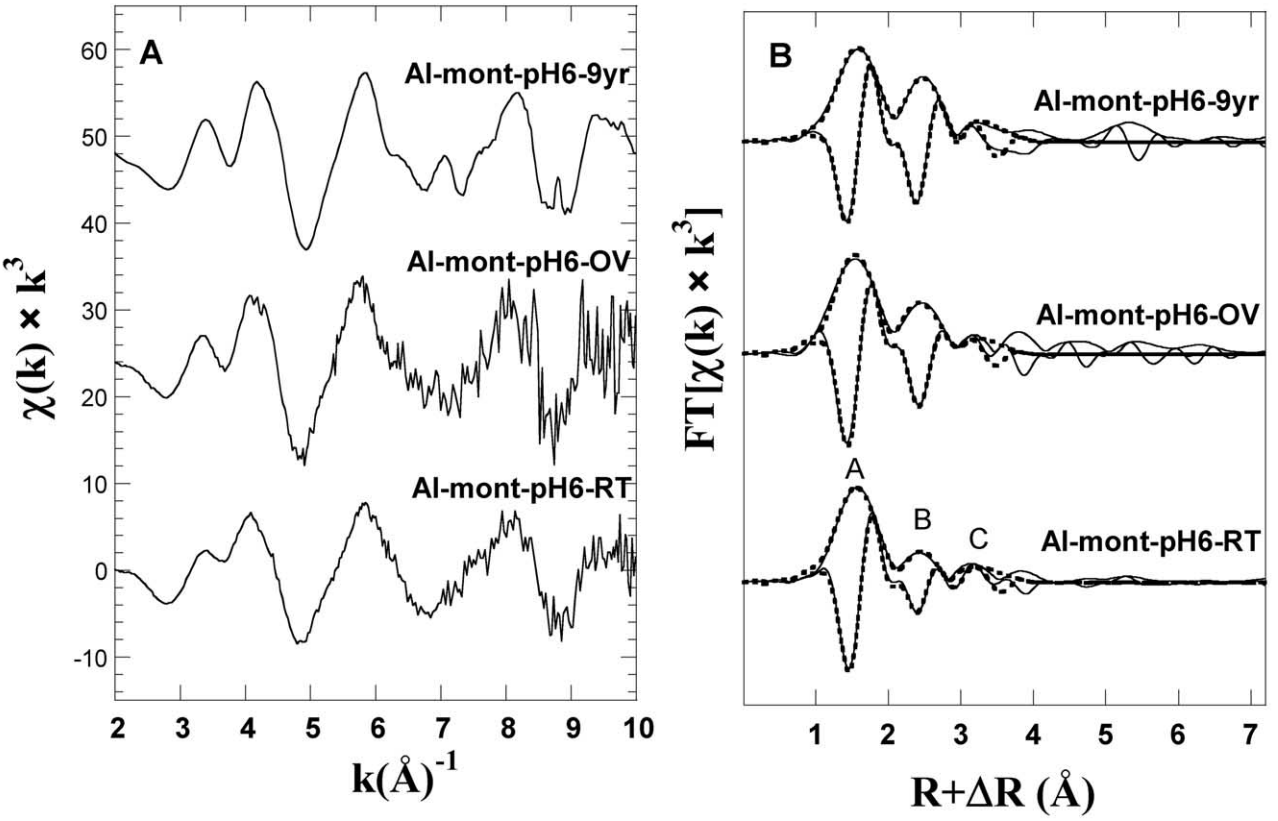

Fig. 2. Effect of reaction time and temperature on (A) the $k^3\chi(k)$ spectra of the pH 6 Ni-sorbed Al-montmorillonite samples, listed as a function of reaction time and temperature, and (B) the Fourier transforms (modulus and imaginary parts). The solid lines indicate the raw data, the dotted lines the best fits. RT = room temperature (≈25°C); OV = oven (80°C).

tributions from neighboring cations. No Ni-Ni pairs could be fitted (Table 2), indicating that no Ni- hydroxide–, Ni-LDH–, or Ni-phyllosilicate–type precipitate was formed under the reaction conditions employed (Dähn et al., 2002). An optimal fit for peak B was obtained by fitting an Al shell at ~3.00 Å. This is at a significantly shorter bond distance than the Ni-Ni backscattering pairs in potential neoformed Ni nucleation phases (e.g., Mont-pH8 (neoformed Ni-phyllosilicate), Table 2). The amplitude of the second RSF peak increased in intensity with increasing reaction time and temperature, with the coordination number ($NN_{Ni\text{-}Al}$) converging to 6 (Table 2). The finding that Ni is surrounded by ~6 Al atoms at ~3.00 Å suggests the inclusion of Ni in an aluminum structure, in which Ni is located in octahedral sites.

A third small peak in the RSFs (C) is mainly caused by single backscattering contributions from further lying oxygen neighbors. The nature of this peak will be corroborated further in the P-EXAFS section (section 3.3). The observation that Ni is already partly included into the Al structure after a month of aging at room temperature shows that the inclusion of Ni into the Al structure is a relatively fast process.

3.2. Quantitative Texture Analysis

The variation of the diffracted intensity of the (004) reflections of two self-supporting clay films are shown in Figure 3, top for the Al-montmorillonite suspension reacted at pH 5 for 1 month at 80°C (Al-mont–pH5–OV) and bottom for the Al-montmorillonite suspension reacted at pH 7 for 9 yrs at room temperature (Al-mont–pH7–9yr). The distribution density of c*-axes perpendicular to the film plane were obtained from the intensities of ρ scans and by averaging for each ρ value the normalized densities of (004) pole figures. Pole densities are expressed as a multiple of a random distribution (mrd.). At ρ = 0°, a maximum with a density value of ~2.1 mrd was observed for the sample reacted at pH 7 (Al-mont–pH7–9yr) and a density value of ~2.2 mrd for the sample reacted at pH 5 (Al-mont–pH5–OV), which indicates that most of the montmorillonite platelets had their (*a,b*) planes aligned parallel to the film plane. These values are lower than the 8–10 mrd values reported for montmorillonite clay films that were not modified with Al (Dähn et al., 2003). The lower values indicate that the Al-modified clay films had a lower texture strength in comparison with the pure clay films, which might have resulted from the alteration of the clay film by the inclusion of Al in the interlayer space.

The experimental ρ scan curves were best-fitted with Gaussians. These fits resulted in a full width at half maximum (FWHM) of 48° for the pH 5 film (Al-mont–pH5-OV) and a FWHM of 36° for the pH 7 film (Al-mont–pH7–9yr). The texture values will be used for the P-EXAFS studies to correct

Table 2. Structural information of powder samples and reference phases derived from EXAFS analysis.

Sample	Γ (μmol/g)[c]	Ni-O			Ni-Al/Ni				Ni-O2			ΔE_0(eV)[a]	%Res[b]	Reference
		*NN**	*R* (Å)[†]	σ^2(Å)^{2‡}		*NN*	*R* (Å)	σ^2(Å)^2		*NN*	*R* (Å)	σ^2(Å^2)		
Bulk EXAFS														
Al-mont–pH6–RT	30.05	6.5	2.02	0.004[d]	Al	5.0	2.97	0.006[d]		14.8	3.89[d]	0.015[d]	−0.05	7.36	
Al-mont–pH6–OV	44.30	6.3	2.02	0.004[d]	Al	5.7	3.00	0.006[d]		13.5	3.89[d]	0.015[d]	−1.82	7.77	
Al-mont–pH6–9yr	35.88	6.3	2.04	0.004[d]	Al	6.9	3.00	0.006[d]		14.7	3.89[d]	0.015[d]	1.59	4.89	
Al-mont–pH8–OV	49.31														
References															
Ni-Al_{13}		5.8	2.05	0.005	Al	5.6	2.95	0.010	O	10.9	3.88	0.010			This study
Ni_{aq}	0.07M	5.7	2.04	0.007											Dähn et al. in prep.
Ni-mont–pH5–OV	144.3	6.3	2.05	0.006											Dähn et al. in prep.
Ni-mont–pH7–9yr	4.0	5.3	2.03	0.005	Al	1.6	3.00	0.006	Si2	4.4	3.27	0.006			Dähn et al. 2003
					Si1	1.9	3.10	0.006	Ni	2.6	3.08	0.008			
Ni-mont–pH8	62.8	5.4	2.04	0.006	Si	4.2	3.26	0.008							Dähn et al. 2002

* Number of neighbors.
† Inter-atomic distance.
‡ Debye-Waller factor.
[a] Inner potential correction.
[b] Fit residual.
[c] Absorber concentration.
[d] Determined by P-EXAFS of pH 5 sample.

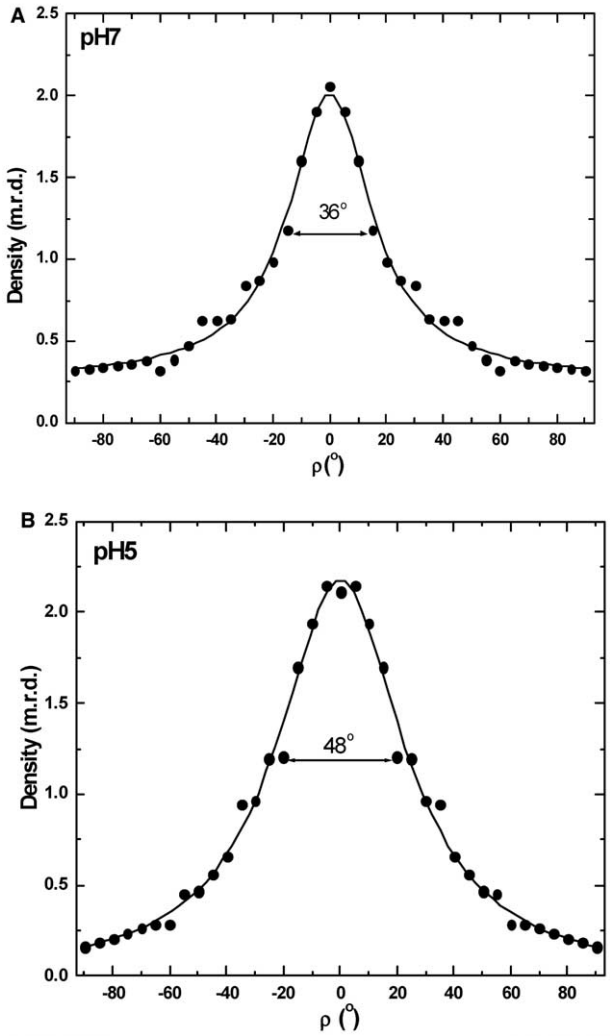

Fig. 3. Integrated radial distribution densities of the c* axes of Al-modified montmorillonite crystals with respect to the normal of the film plane (ρ = 0°) for (top) pH 5 Ni-reacted Al-montmorillonite and (bottom) pH 7 Ni-reacted Al-montmorillonite.

the number of neighbors and the experimentally determined β angles for the imperfect orientation of the film (section 3.3). The fact that the mosaic spread of the particle distribution or the FWHM was smaller for the 9-year-aged pH 7 sample compared to the 1-month-aged pH 5 sample indicates that the clay particles were much better oriented in the pH 7 sample. This difference in orientation of the clay particles was not caused by differences in the experimental set up (repetitions on clay mineral films prepared under the same conditions showed the same difference in FWHM—data not shown), but rather resulted from intrinsic differences between the two clay films.

Both films have contributions that do not completely vanish at ρ = 90° (mrd >0, Fig. 3). This finding suggests that a certain percentage of the particles in the experimental system are randomly oriented (20% and 30% in the pH 5 and pH 7 samples, respectively). This random orientation is absent when clay films were produced from Ni-treated montmorillonite (Dähn et al. 2003). If the randomly oriented particles contain

Ni, the presence of nonoriented material will influence the P-EXAFS spectra. This will be visible as a decreased angular dependence of the $k^3\chi(k)$ spectra compared to spectra of highly oriented clay films. However, the lower crystallite dispersion present in the oriented part of sample pH 7 could partly compensate for the effect of the decreased angular dependence.

Based on the results of the quantitative texture analysis, it can be concluded that two fractions exist in the clay film that have a different texture. For example, the pH 7 sample is composed of ~30% of randomly oriented particles and ~70% of oriented crystallites having a gaussian distribution shape of 36° FWHM. We will come back to this when discussing the P-EXAFS data (section 4.1).

3.3. P-EXAFS of pH 5 and pH 7 Self-Supporting Clay Films

Polarized EXAFS was used to unequivocally determine the structure of sorbed/incorporated Ni and to elucidate the orientation of its surrounding shells with respect to the clay mineral layering. Figures 4a and 5a show the angular dependence of the k^3-weighted $\chi(k)$ P-EXAFS spectra of the Ni-treated Al-montmorillonite clay films prepared at pH 5 and 7 (Al-mont–pH5–OV and Al-mont–pH7–9yr), respectively. With increasing α angle, the splitting of the first oscillation, as well as the intensity of the second oscillation, decreases. These changes in spectral intensity indicate that the coordination chemistry of Ni is anisotropic and, more specifically, that its local structure is oriented with respect to the layering of the clay film. All spectra contain several isobestic points distributed over the whole k range, for which $\chi(k)$ is independent of k. The fact that all the individual $\chi(k,\alpha)$ spectra precisely cross at the same value in these points provides strong proof of the reliability of our P-EXAFS data quality and analysis.

The corresponding RSFs and their best fits are displayed in Figures 4b and 5b. The figures show that the fits match the experimental data well for both the real and the imaginary parts. Furthermore, the figures illustrate that the amplitude of the imaginary part is strongly dependent on the α angle. Similar FT peaks as in the EXAFS spectra of the pH 6 Ni sorption samples (Fig. 1) were observed at $R + \Delta R$ of 1.6 Å, 2.5 Å, and 3.2 Å (marked A, B, and C). The position of peak A (Ni-O contribution) is invariant with varying α angle, whereas its amplitude slightly decreases with increasing α angle. The amplitude of peak B (Ni-Al contribution) strongly decreases with increasing α angle, and a small third peak, labeled C (Ni-O2 contribution), is present at all angles. A fourth peak, labeled D, between $R + \Delta R$ ~5.0–6.0 Å is only present in the pH 7, 9-year-aged sample and shows a decreasing amplitude with increasing α angle. No attempts were made to fit this last peak. Previous research of Zn and Ni sorption onto Al hydroxides has attributed this small peak to multiple scattering from contributions of Al atoms (Yamaguchi et al., 2002; Roberts et al., 2003).

Structural parameters derived from multishell fitting of the Al-mont–pH5–OV and Al-mont–pH7–9yr samples in *R*-space are reported in Table 3. To reduce the number of fit parameters, $R_{\text{Ni-O}}$, $\sigma^2_{\text{Ni-O}}$, $R_{\text{Ni-Al}}$, $\sigma^2_{\text{Ni-Al}}$, and ΔE_o were determined at $\alpha = 35°$ and then held fixed at $\alpha \neq 35°$. $R_{\text{Ni-O2}}$ and $\sigma^2_{\text{Ni-O2}}$ were determined at $\alpha = 10°$. It follows that the observed decrease in peak intensity with increasing α angle (as shown in Figs. 4b and 5b) corresponds to a reduction of the number of neighbors, i.e., NN^{EXAFS}_{Ni-O} decreases from 6.8 (pH 5) and 6.2 (pH 7) at $\alpha = 10°$ to NN^{EXAFS}_{Ni-O} of 4.8 and 4.5 at $\alpha = 80°$. To a larger extent, NN^{EXAFS}_{Ni-Al} decreases from 7.5 to 2.4 in the pH 5 film and from 8.1 to 2.0 in the pH 7 film (Table 3). The decrease of NN^{EXAFS}_{Ni-Al} with increasing α implies that $\beta_{\text{Ni-Al}}$, the angle between the film normal and the vector connecting the X-ray-absorbing atom (Ni) to the backscattering atom (Al), is larger than 54.7° (Dähn et al., 2002).

The angle, β, between the film normal and the vector connecting the X-ray absorbing atom (Ni) to the backscattering atoms (Al), can be experimentally determined from the variation of the NN as a function of α (Dähn et al., 2003). The exact bond angle between the Ni-Al pairs and the layering of the montmorillonite clay particles can be calculated by rewriting Eqn. 1 as a function of $\cos^2\alpha$:

$$\frac{NN^{EXAFS}_{j,\alpha}}{NN^{CRYST}_{j}} = \frac{I_{ord}}{2}(3 - 9\cos^2\beta^{cryst}_j)\cdot\cos^2\alpha + 3I_{ord}\cos^2\beta^{cryst}_j + 1 - I_{ord} \quad (3)$$

or

$$\frac{NN^{EXAFS}_{j,\alpha}}{NN^{CRYST}_{j}} = a\cdot\cos^2\alpha + b \quad (4)$$

where a and b are regression coefficients. These can be obtained by plotting NN^{EXAFS}_{Ni-Al} vs. $\cos^2\alpha$ as shown in Figures 4c and 5c for the Al-mont–pH5–OV sample and the Al-mont–pH7–9yr samples, respectively ($r^2 > 0.999$). β^{cryst}_j can be obtained from:

$$\beta^{cryst}_j = \arccos\sqrt{\frac{3 - 2a/I_{ord}}{9}} \quad (5)$$

which yields $\beta_{\text{Ni-Al}} = 69°$ for the pH 5 film and $\beta_{\text{Ni-Al}} = 72°$ for the pH 7 film, assuming a perfectly ordered film ($I_{ord} = 1$). As discussed in section 3.2, some of the montmorillonite platelets were tilted with respect to the film plane. One can correct for this particle disorder by calculating I_{ord}, the function that accounts for the particle disorder, using Eqn. 2 and using the half width of half maximum (HWHM) of the mosaic spread of the clay particles of the film plane. Eqn. 2 was solved numerically because the integral in the numerator has no analytical solution (Manceau and Schlegel, 2001). The resulting values for I_{ord} are 0.81 for the pH 7 film and 0.69 for the pH 5 film. These results show that the Al-mont–pH7–9yr film had a much better alignment of the clay particle platelets as the Al-mont–pH5–OV film.

This better alignment is also reflected in the structural parameters listed in Table 3. The Al-mont–pH7–9yr sample had lower Debye-Waller factors compared to the Al-mont–pH5–OV sample, as a result of the reduced disorder. Taking the calculated I_{ord} values into account, the corrected β values are $\beta^{\text{real}} = 77°$ for the pH 5 film and $\beta^{\text{real}} = 79°$ for the pH 7 film. These values indicate that the Ni-Al pairs are oriented parallel to the montmorillonite film plane (the slight deviation of α from 90° will be discussed in section 4.1). The finding that the Ni-Al pairs are parallel to the film plane indicates that the

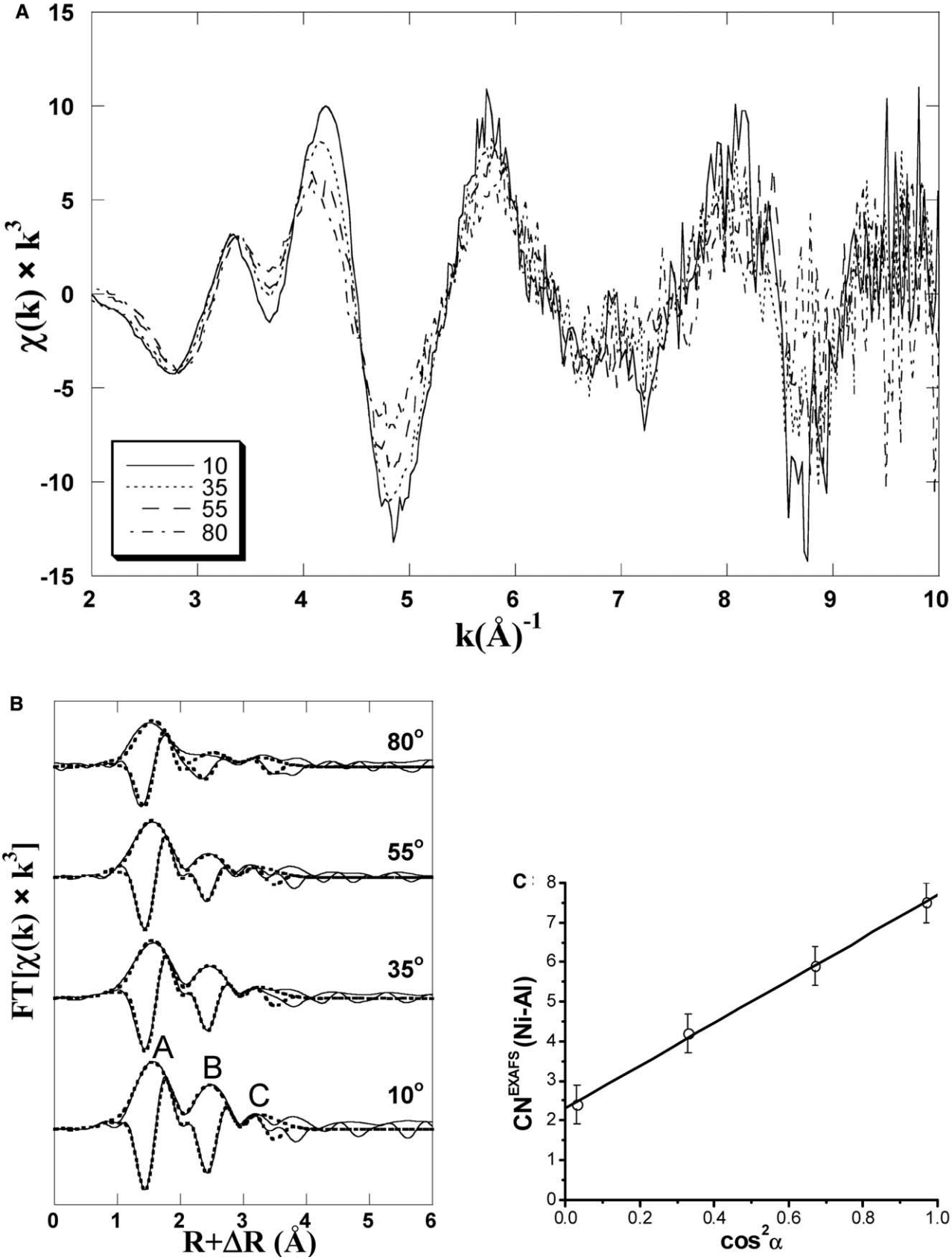

Fig. 4. (A) k^3-weighted Ni K-edge P-EXAFS spectra of the Ni-reacted Al-modified montmorillonite film at α angles of 10°, 35°, 55°, and 80° (19.6 μmol/g at pH 5, 1 month reaction time). (B) Polarization dependence of the Fourier transforms (modulus and imaginary parts) of the pH 5 Ni-reacted Al-montmorillonite. The solid lines indicates the raw data, the dotted lines the best fits. (C) Angular dependence of $NN_{\text{Ni-Al}}$. Open circles indicate experimental data, and the solid line is the linear regression ($R = 0.999$). $NN_{\text{Ni-Al}} = 5.37 \cos^2\alpha + 2.31$. The uncertainty on NN is estimated to be ± 0.5.

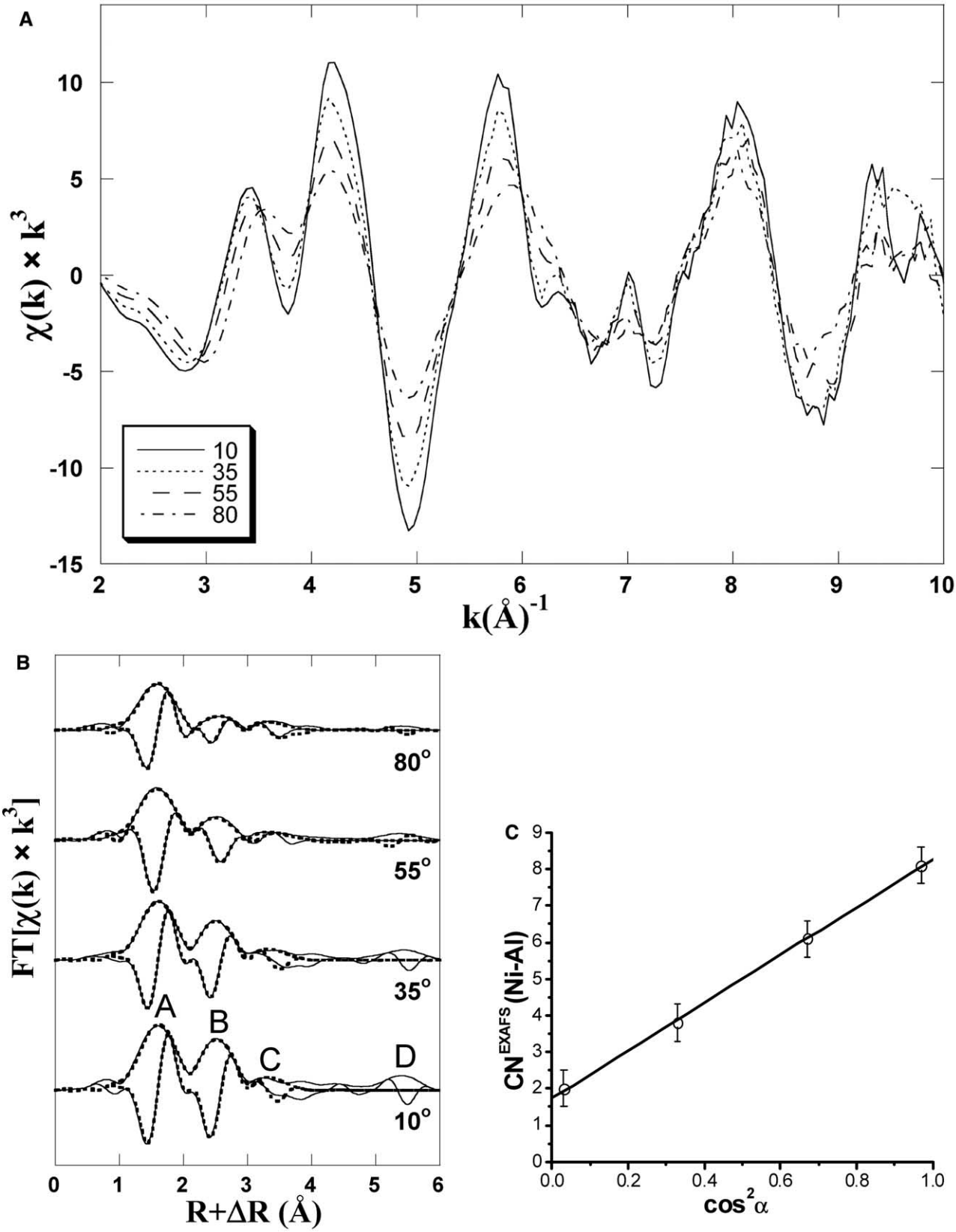

Fig. 5. (A) k^3-weighted Ni K-edge P-EXAFS spectra of the Ni-reacted Al-modified montmorillonite film at α angles of 10°, 35°, 55°, and 80° (48.5 μmol/g at pH 7, 9 yrs reaction time). (B) Polarization dependence of the Fourier transforms (modulus and imaginary parts) of the pH 7 Ni-reacted Al-montmorillonite. The solid lines indicates the raw data, the dotted lines the best fits. (C) Angular dependence of $NN_{\text{Ni-Al}}$. Open circles indicate experimental data, and the solid line is the linear regression ($R = 0.999$). $NN_{\text{Ni-Al}} = 6.52 \cos^2\alpha + 1.74$. The uncertainty on NN is estimated to be ± 0.5.

Table 3. Structural data, derived from polarized EXAFS analysis of the pH5 Ni-reacted Al-modified montmorillonite and the pH7 Ni-reacted Al-modified montmorillonite samples.

	Ni-O			Ni-Al			Ni-O				
α	NN*	R (Å)†	σ^2(Å)^{2}‡	*NN*	*R* (Å)	σ^2(Å)^2	*NN*	*R* (Å)	σ^2(Å)^2	ΔE_0(eV)§	%Res!
Al-mont–pH5–OV											
10°	6.8	2.03[a]	0.004[a]	7.5	3.01[a]	0.006[a]	18.0	3.89	0.015	−0.62[a]	6.75
35°	5.9	2.03	0.004	5.9	3.01	0.006	12.9	3.89[b]	0.015[b]	−0.62	7.68
55°	5.8	2.03[a]	0.004[a]	4.2	3.01[a]	0.006[a]	11.5	3.89[b]	0.015[b]	−0.62[a]	9.12
80°	4.8	2.03[a]	0.004[a]	2.4	3.01[a]	0.006[a]	10.8	3.89[b]	0.015[b]	−0.62[a]	21.73
	4.8	2.03[a]	0.004[a]	2.4	2.96	0.006	10.8	3.89	0.015	−0.62[a]	
											14.80
Al-mont–pH7–9yrs											
10°	6.2	2.05[a]	0.003[a]	8.1	3.03[a]	0.004[a]	21.3	3.92	0.012	−1.62[a]	6.81
35°	5.6	2.05	0.003	6.1	3.03	0.004	18.5	3.92[b]	0.012[b]	−1.62	7.38
55°	5.0	2.05[a]	0.003[a]	3.8	3.03[a]	0.004[a]	15.1	3.92[b]	0.012[b]	−1.62[a]	7.20
80°	4.5	2.05[a]	0.003[a]	2.0	3.03[a]	0.004[a]	11.9	3.92[b]	0.012[b]	−1.62[a]	10.40

[a] Fixed to the value determined at $\alpha = 35°$.
[b] Fixed to the value determined at $\alpha = 10°$.
* Number of neighbors.
† Inter-atomic distance.
‡ Debye-Waller factor.
§ Inner potential correction.
! Fit residual.

newly formed Ni-doped aluminum mineral is oriented parallel to the clay mineral layering and most likely formed in the interstitial space of the montmorillonite.

A small third peak at $R + \Delta R = 3.6$ Å is visible in the RSFs of all Ni-reacted Al-modified montmorillonite spectra. This peak could be fitted in the P-EXAFS spectra with a single scattering Ni-O path at around 3.9 Å. This Ni-O2 bond distance corresponds to a further-distanced O shell in the gibbsite monolayer. The existence of such further-distanced metal-O shells has been reported before for Zn included into the octahedral layers of hectorite (Schlegel et al., 2001b) and for Fe in nontronite, an iron containing smectite (Manceau et al., 1998). In the study by Manceau et al. (1998), the coordination of Fe in the octahedral layers of nontronite was investigated using Fe K-edge P-EXAFS and ab initio modeling. The authors suggested that the single scattering Fe-O path at $R = 3.74$–3.83 Å resulted from oxygen ligands from neighboring edge-sharing Fe atoms.

Because the presence of further distanced Ni-O backscattering pairs has a strong influence on the structural parameters derived for the Ni-Al shell, they had to be included into the fit approach used in this study (Tables 2 and 3). Similar to Schlegel et al. (2001b) and Manceau et al. (1998), we used a single scattering Ni-O2 backscattering path to account for the presence of further-distanced Ni-O backscattering pairs. In reality, however, we must assume that there is a spread of Ni-O2 bond distances in the Ni-doped Al structure that is similar to the spread of Al-O2 bond distances in gibbsite (Saalfeld and Wedde, 1974). Consequently, this approach results in an average of Ni-O2 bond distances, Debye-Waller factors, and Ni-O2 nearest neighbors that are a factor two too high (see Table 3).

As mentioned earlier, the Ni-O2 coordination shell is responsible for the characteristic strong splitting of the first oscillation in the $\chi(k^3)$ spectra of the Ni-reacted Al-modified montmorillonite samples (see section 3.1). As shown in Figure 6, the splitting of this oscillation and some other spectral features of the pH 7 P-EXAFS spectrum collected at 35° could not be reproduced when only contributions from O and Al in the EXAFS simulation were assumed. However, when a single scattering Ni-O2 backscattering path was included into the EXAFS simulation, all features were successfully reproduced (Fig. 6). This indicates that the characteristic splitting of the first EXAFS oscillation is caused by further-distanced O shells at 3.7–3.9 Å and not by Al as reported in the case of metal sorption to gibbsite (Yamaguci et al., 2002; Manceau et al., 2000; Roberts et al., 2003). However, the contribution of multiple scattering paths can not be excluded.

3.4. Competition of Other Ni Uptake Mechanisms

So far, we have shown that at pH 5–7 Ni is predominantly included into a newly formed Al phase, which is partly formed into the interlayer space of the montmorillonite.

At higher pH (e.g., pH 8), the experimental conditions are such that solubility limits for neoformed Ni nucleation phases (e.g., Ni-phyllosilicates, a mixed Ni-Al layered double hydroxide (LDH), and $Ni(OH)_2$)) are potentially reached (Hummel and Curti, 2003) and precipitation should take over as the dominant Ni uptake mechanism.

Indeed, Figure 7a shows that the spectrum of the pH 8 sample (Al-mont–pH8–OV) contains features in the $k^3\chi(k)$ spectra, that are clearly not present in the spectrum of the Ni-reacted Al-modified montmorillonite suspension (Al-mont–pH6–OV, see arrows). These features are signatures of the phyllosilicate precipitate formed in the presence of montmorillonite (Mont-pH8).

Both the formation of a Ni-Al interlayer phase and the formation of a Ni-phyllosilicate phase contribute to the Al-mont–pH8–OV spectrum. Thus, a linear fitting approach was used to determine the relative contributions of the different Ni uptake modes in to the Al-mont–pH8 spectrum (Fig. 7b and c). Multiple linear combinations were tested using the reference

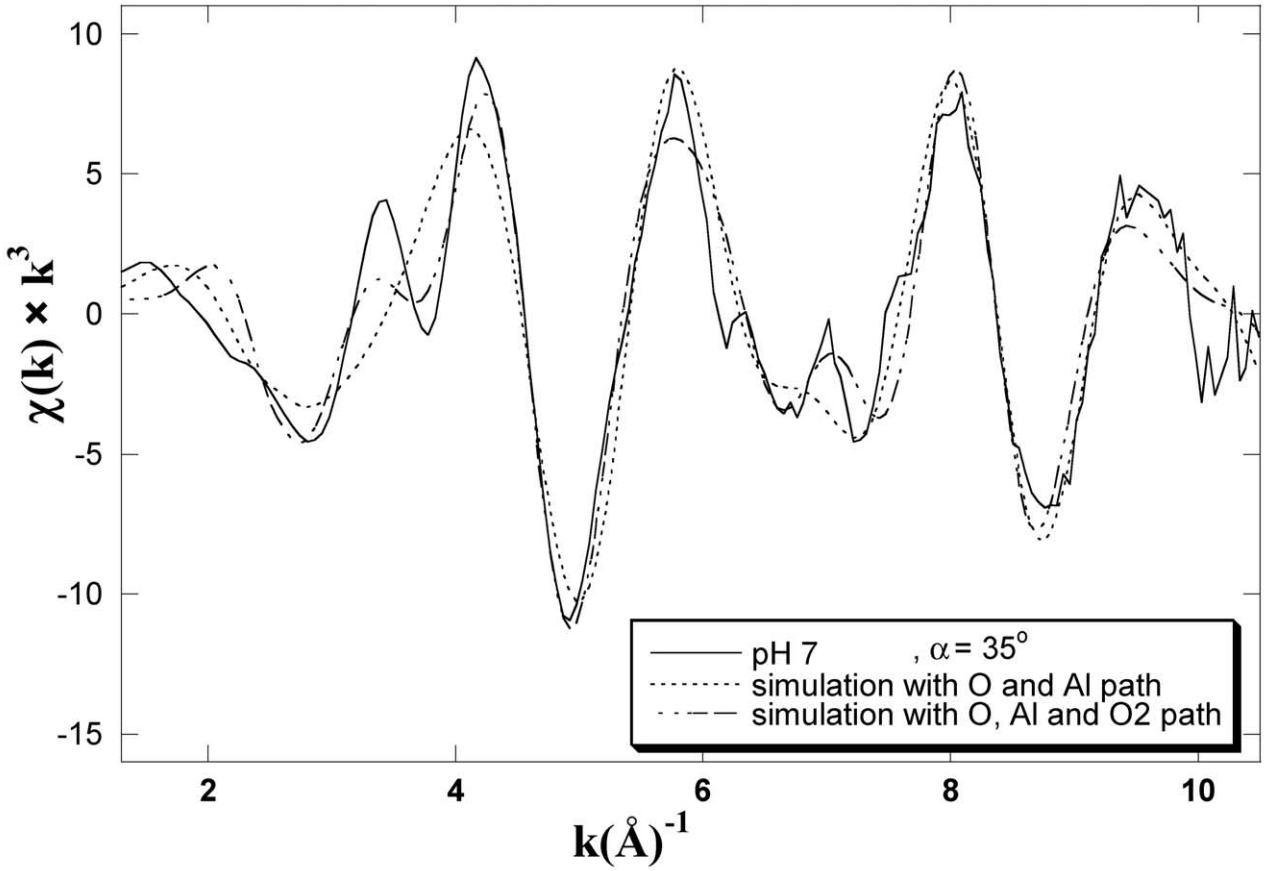

Fig. 6. k^3-weighted Ni K-edge P-EXAFS spectra of the Ni-reacted Al-modified montmorillonite film at α angle of 35, and two simulations, one with a Ni-O and Ni-Al scattering path and one with an additional Ni-O2 scattering path.

spectra listed in Figure 1. For comparison we first tried to simulate the Al-mont–pH8–OV spectrum with only one component. In this case the best spectral agreement was reached using the Ni-reacted Al_{13} reference sample (fit residual = 0.184; Fig. 7b).

Although the component simulation reproduced the spectral phase well, it did not reproduce the characteristics in the first oscillation, justifying the addition of a second component to the fit. The best two-component fit was obtained with 65% Al_{13} and 34% Mont-pH8 and improved the fit by more than 50% (Res = 0.082, Fig. 7c). As inferred from Figure 7c, both a Ni precipitate and Ni in the newly formed Al-phase contribute to the Al-mont–pH8–OV spectrum. The amplitude and the phase of the Al-mont–pH8–OV spectrum are well reproduced by this two-component fit, although there are still notable differences especially in the first oscillation.

Nevertheless, the results clearly indicate that although the neoformation of a Ni-phyllosillicate–like phase does occur in the experimental system, the uptake of Ni is still dominated by the inclusion of Ni into an interstitial Al phase.

4. DISCUSSION

4.1. Proposed Sorption Mechanism

Our investigation of the molecular scale uptake mechanism of Ni by Al-modified montmorillonite was initiated by a macroscopic metal-uptake study of Lothenbach et al. (1997), in which a much larger Ni uptake was observed in the Al-modified montmorillonite compared to unmodified montmorillonite.

Using powder EXAFS, we further investigated a sample prepared by Lothenbach et al. (1997) that reacted with a Ni solution for 9 yrs (see section 3.1). The EXAFS investigations showed that Ni "sorbed" onto Al-modified montmorillonite has a local coordination environment (~6 O at 2.04 Å and ~6 Al at 3.01 Å) that indicates the incorporation of Ni into vacant octahedral sites of an aluminum structure. The EXAFS findings presented within this manuscript support the findings from a bulk EXAFS study on the Ni uptake mechanism by Al-modified montmorillonite (Furrer et al., 2001). In the earlier study, a 5-year-aged sample was investigated and the EXAFS data suggested that Ni is rather associated to an aluminum phase than to the clay itself. However, any conclusions on the orientation and structural link of the aluminum phase and the montmorillonite clay platelets could not be derived from the bulk EXAFS analysis.

Based on the angular dependence of the P-EXAFS spectra and the structural parameters obtained by data analysis, it could be demonstrated that a Ni-doped gibbsite is being formed in the Al-montmorillonite suspensions, where Ni occupies the vacant octahedral sites. Gibbsite has one out of three octahedral sites vacant and is the most stable and likely Al mineral to form

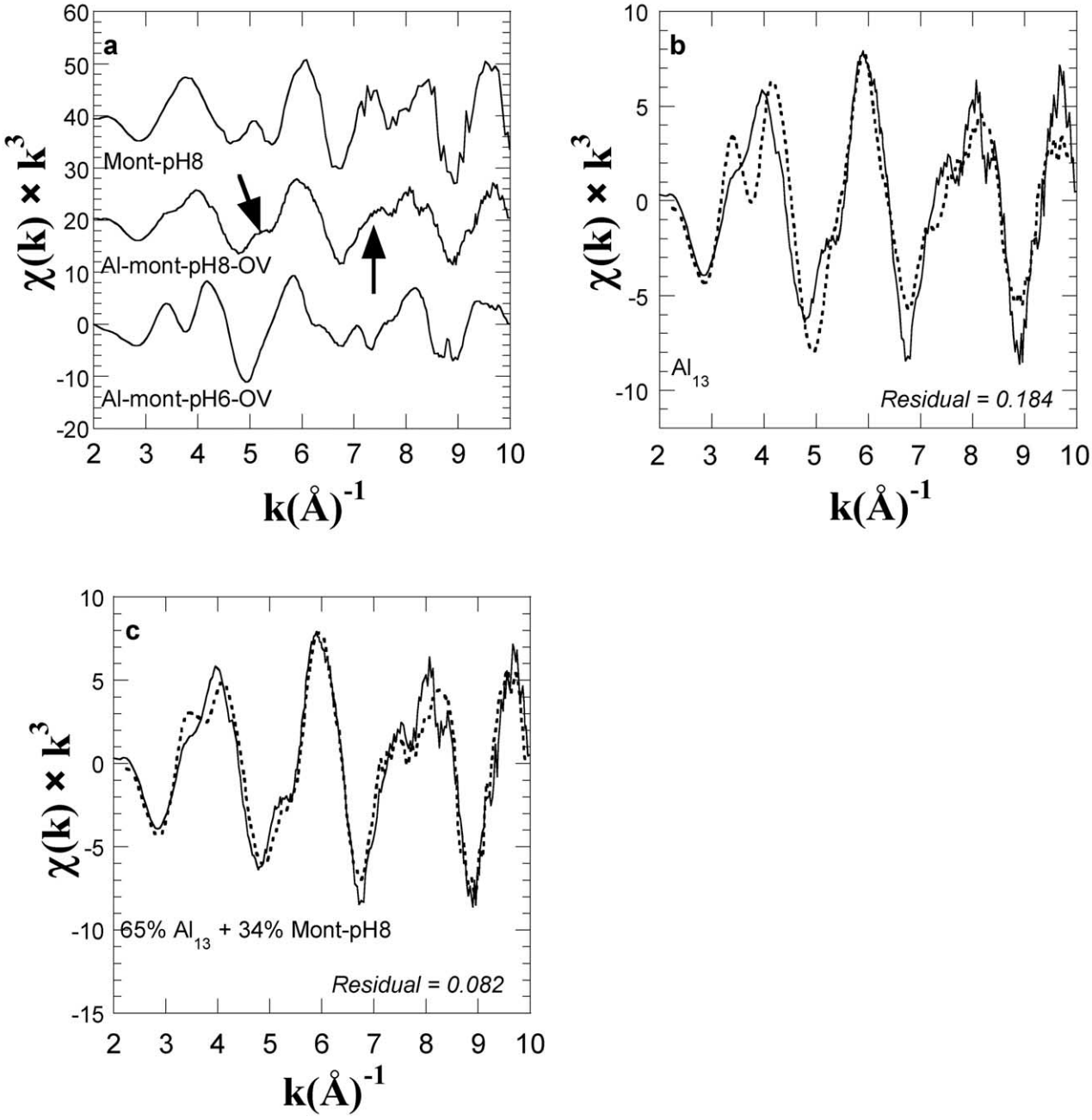

Fig. 7. (a) k^3-weighted Ni K-edge EXAFS spectra of the pH 8 montmorillonite sample, the Ni-reacted Al-mont–pH6 sample and the Mont-pH8 sample. (b–c) Linear combination fits, with (b) a one-component fit, (c) a two-component fit. The solid lines indicate the Al-mont–pH8 spectrum, and the dotted lines indicate the fits.

under the reaction condition employed in this study and in the study by Lothenbach et al. (1997).

P-EXAFS measurements on oriented self-supporting Ni-reacted Al-modified montmorillonite films show a pronounced angular dependence that allows in-plane and out-of-plane contributions to be distinguished. From the variation of the *NN* as a function of α, the angle between the film normal and the vector connecting the x-ray–absorbing Ni atom to the backscattering Al atoms was determined to be ~80°, indicating that the Ni-doped gibbsite is oriented parallel to the montmorillonite clay particles. This finding suggests that a Ni-doped gibbsite is either formed in the interstitial space or at edge sites of the montmorillonite. Based on published XRD *d*-spacings of ~16 Å for the interstitial space of a metal-reacted Al-modified montmorillonite (Lothenbach et al., 1997), it is concluded that most of the Ni-doped gibbsite is formed in the interstitial space of the montmorillonite. The thickness of the newly formed Ni-doped gibbsite can never exceed that of a monolayer. Gibbsite in the interlayer can be present in the form of a monolayer or as distinct gibbsite "islands" similar to pillared

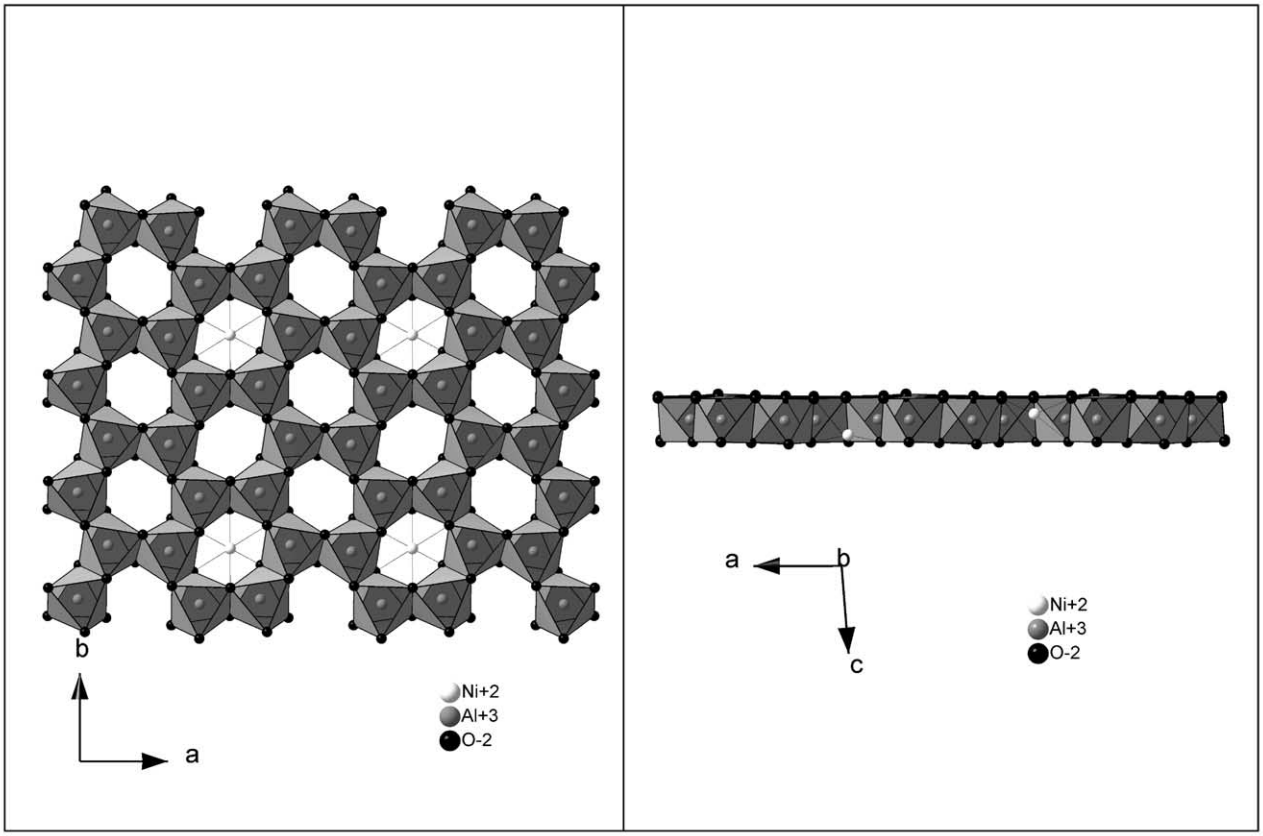

Fig. 8. Proposed structure for the interstitial Ni-doped gibbsite monolayer. Note that Ni atoms are not in plane with the Al atoms.

clays. P-EXAFS can not distinguish between these two. The idea of gibbsite "islands" forming within the interlayer when preparing the clays has the added benefit that Ni can easily diffuse through the interlayer and sorb to the gibbsite "islands." Rearrangement of the gibbsite "islands" with sorbed Ni will then form a more extended gibbsite monolayer, with Ni included in the structure. The results presented in Figure 2 and Table 2, where an increase of Ni-Al NN was reported with increasing reaction time, support this scenario.

Owing to substitutions of Ni^{2+} in the vacant octahedral sites of the gibbsite, this monolayer will have a net positive charge. This positive charge of the gibbsite monolayer compensates the permanent negative charge of the clay layers.

The slight deviation of α from 90° (the bond angle indicating a parallel orientation of the Ni-Al bond vector with the montmorillonite layering) suggests that Ni is not placed exactly in the gibbsite monolayer, but slightly above or below the gibbsite monolayer. This hypothesis is also supported by the Ni-Al bond distances observed in this study. If Ni is placed exactly in the unoccupied octahedral sites of the gibbsite one might expect that Al-Al bond distances and Ni-Al bond distances are equal. However, Al-Al bond distances reported in gibbsite are 2.95 Å (Saalfeld and Wedde, 1974), whereas our measured Ni-Al bond distance is 3.01 Å. A distance of 3.01 Å is exactly the calculated Ni-Al bond length, assuming that the Ni-Al bond vector is at an angle of 10° with respect to the Al-Al bond vector. The structural displacement of divalent Ni from the gibbsite monolayer puts the positively charged Ni closer to the negative charge of the clay mineral layers.

Based on these considerations, we propose a structure for Ni-reacted Al-modified montmorillonite as depicted in Figure 8, in which Ni is placed slightly above or below the vacant octahedral sites of the gibbsite structure.

We observed that the peak at $R + \Delta R = 2.5$ Å (labeled B in Figs. 2b, 4b, and 5b) was caused by Ni-Al backscattering. This means, for the interstitial Ni-doped monolayer gibbsite, that this peak is most pronounced when the electric field vector, ε, is parallel to the film plane, i.e., at $\alpha = 10°$. This peak should disappear when ε is perpendicular to the film plane, i.e., at $\alpha = 80°$. However, we could still fit up to 2 Al at $\alpha = 80°$ in the pH 5 and pH 7 films (Table 3). There are two processes that contribute to the fact that the Ni-Al *NN* does not come close to 0 at 80°. First, as discussed before, Ni is lying slightly above and below the vacant sites of the monolayer gibbsite. Thus the Ni-Al peak does not completely diminish in the out-of-plane direction. Second, a significant portion of Ni is not included in the gibbsite monolayer, but in an Al phase formed outside the interlayer of the montmorillonite. The texture analysis in section 3.2 showed that 30% of the Al-modified montmorillonite particles are randomly oriented, whereas in the absence of aluminum all montmorillonite particles are oriented (Dähn et al., 2003). This finding suggests that part of the Ni-bearing aluminum phase is formed outside the montmorillonite interlayer. If this Al phase is randomly oriented, then the Ni-Al *NN*

will have a contribution independent of the angle of the incoming beam.

Further evidence for Ni bound to a randomly oriented Al phase comes from a comparison of the fitting parameters obtained for the pH 5, 80°, P-EXAFS spectrum (Table 3) and the fitting parameters obtained for the Ni-Al_{13} reference phase (Table 2). Similarly to earlier P-EXAFS studies with smectites, we fixed the Debye-Waller factors and the bond distances of the Ni-Al shell to the values obtained at $\alpha = 35°$ (Dähn et al., 2002, 2003). With this fitting approach, we determined a Ni-Al bond distance of 3.01 Å. Though this fitting approach worked reasonably well at α of 10°, 35°, and 55°, the fit residual for 80° is clearly bigger (Res = 21% compared to Res = 8% for the other α angles). When the Ni-Al bond distances and the Debye-Waller factors were allowed to vary, the Ni-Al *NN* and the Debye-Waller factor changed only slightly. However, despite the errors associated with the Ni-Al bond distance, we see that the Ni-Al bond distance decreased from 3.01 to 2.96 Å and the fit residual significantly improved from 21% to 14%. A Ni-Al bond distance of 2.96 Å favorably compares to the typical Ni-Al bond distances (2.95 Å) for Ni binding to Al-(hydr)oxides (Table 2, with Al_{13} used as a proxy for Al-(hydr)oxides) (Yamaguci et al., 2002). The reason that longer Ni-Al distances are found for Ni included into the monolayer gibbsite, is that Ni is not placed within the gibbsite layer, but slightly above and below the vacant octahedral sites.

The number of neighbors (*NN*) for Ni-Al at $\alpha = 80°$ can be estimated by taking the Ni fraction both outside and inside the montmorillonite interlayer into account. With ~30% of the material (with a Ni-Al *NN* of 6, as in Ni-Al_{13}) randomly oriented (see texture analysis in section 3.2), and 70% oriented parallel to the self-supporting film (with a Ni-Al *NN* of 0 at $\alpha = 80°$), the measured *NN* in the P-EXAFS spectrum at 80° should be 6*0.3 = 1.8, which is fairly close to the values reported in Table 3.

4.2. Structural Relationship to Similar Layered Oxides

The newly identified Ni-doped gibbsite monolayer formed in the interstitial space of montmorillonite minerals shares structural resemblances with other layered minerals containing Al or Mg octahedral layers. For example, a similar type of Ni sequestration mechanism in a gibbsite-like monolayer was observed in lithiophorite, which is a MnO_2-$Al(OH)_3$ mixed layered oxide (Manceau et al. 1987, 2000). In the EXAFS spectra obtained from Ni-containing lithiophorite, a strong split of the first oscillation was also observed, which was attributed to the presence of "light" Al atoms in the second coordination shell. Similar to montmorillonite clay layers, the Mn-bearing layers are negatively charged, owing to Mn^{3+} for Mn^{4+} substitution. This negative charge is compensated by a positively charged gibbsite layer in which Ni, Cu, and Zn can be placed in the vacant octahedral sites.

The inclusion of Ni into the octahedral layers of clay minerals, which consist of either dioctahedral Fe or Al (similar to gibbsite) or trioctahedral Mg layers (Sparks, 2003) should share some structural features similar to the interstitial Ni-doped gibbsite monolayer. Therefore, some spectral similarities, such as a weak splitting of the first oscillation and the presence of a weak second O peak in the FT spectra, are expected. For example, an EXAFS study by Schlegel et al. (2001b), where Zn-containing hectorite was synthesized (hectorite is, like montmorillonite, a 2:1 clay mineral, but contrary to montmorillonite the octahedral layer consists of Mg octahedra with no vacant octahedral sites), indeed showed a strong splitting of the first oscillation in the $k^3\chi(k)$ spectra upon inclusion of Zn in the octahedral layering.

4.3. Geochemical Implications for Metal Stability

EXAFS and P-EXAFS data presented here provide a basis for the design and possible use of Al-modified montmorillonites for engineering purposes, such as liner material for waste deposits or backfill material for low radioactive waste. The inclusion of Ni into a mineral phase formed in the interlayer of the clay mineral, as identified here, potentially leads to a less accessible and therefore more stable metal fraction. We have shown that the inclusion of Ni into a gibbsite monolayer is a relatively fast process occurring within a time span of months. The observation of a better texture strength in the longer-aged sample compared to a sample aged for a month indicates that significant reordering of the interlayer mineral phase takes place, possibly transforming a more amorphous phase into a more crystalline phase.

This better crystallinity of the interlayer material is also reflected in the structural parameters listed in Table 3. The Al-mont–pH7–9yr sample had much lower Debye-Waller factors compared to the Al-mont–pH5–OV sample, as a result of the reduced disorder. This might explain the observed increased stability with aging time of the sorbed metal upon sudden acidification (Lothenbach et al., 1999).

Other cations with similar ionic radii, such as Co, Cu, and Zn, should similarly be incorporated in the interstitial gibbsite monolayer. The inclusion and subsequent stabilization of Cu and Zn by Al-modified montmorillonite has been observed earlier (Lothenbach et al., 1997, 1999). The incorporation of Zn into the Al-hydroxy interlayer of smectites has also been proposed as a sequestration mechanism of Zn in acidic smelter-contaminated soils (Scheinost et al., 2002). However, that sequestration mechanism was based solely on a Zn-Al coordination number of 6 that they obtained by EXAFS investigations of a sample that underwent 6 sequential extractions. Thus a distinct proof for the formation of a Zn-containing Al-hydroxy smectite at the acidic conditions of the soil seems to be warranted. The much lower Zn-Al *NN* observed after the first extraction steps suggests that Zn is more likely to be adsorbed to Al compounds such as gibbsite. Moreover, polynuclear compounds, such as Al_{13}, are very likely to be formed under such acidic soil conditions (and could potentially be preferentially formed by the different sequential extraction agents) (Furrer et al., 2002). Metal-sorbed Al_{13} shares the same spectral features as metal-sorbed Al-hydroxy interlayered smectites. It is unlikely that all other mineral phases would dissolve with more extraction steps, but the clay mineral stays in the remaining fraction. Especially because clay minerals dissolve at these low soil pHs and polynuclear Al species form (Furrer et al., 1993). As demonstrated in this study, only the use of P-EXAFS can unequivocally prove the formation of this metal-doped gibbsite monolayer or gibbsite "islands" in the interstitial space of clay minerals.

Acknowledgments—We are grateful to the staff at DUBBLE and SNBL for their support during the EXAFS measurements at the European Synchrotron Radiation Facility (ESRF), Grenoble, France, and the ESRF for the provision of beamtime. This research was funded by Top Nano 21 of the Swiss KTI innovation research program. Daniel Chateigner acknowledges the Délégation Régionale à la Recherche et à la Technologie for financial support. Thanks are extended to Dr. F. Farges and two anonymous reviewers for their helpful comments and suggestions to the original manuscript.

Associate editor: G. Sposito

REFERENCES

Ankudinov A. L., Ravel B., Rehr J. J., and Conradson S. D. (1998) Real-space multiple-scattering calculation and interpretation of x-ray-absorption near-edge structure. *Phys. Rev. B* **58,** 7565–7576.

Baeyens B. and Bradburry M. H. (1995) A quantitative mechanistic description of Ni, Zn and Ca sorption on Na-montmorillonite. Part I: Physico-chemical characterisation and titration measurements. PSI Bericht No. 95-10. Paul Scherrer Institut, Villigen, Switzerland, and Nagra Technical Report NTB95-04, Nagra, Wettingen, Switzerland.

Bellotto M., Rebours B., Clause O., Lynch J., Bazin D., and Elkaim E. (1996) A reexamination of hydrotalcite crystal chemistry. *J. Phys. Chem.* **100,** 8527–8535.

Bunge H. J. and Esling C., eds. (1982) *Quantitative Texture Analysis.* Deutsche Gesellschaft für Metallkunde.

Dähn R., Scheidegger A. M., Manceau A., Schlegel M. L., Baeyens B., Bradburry M. H., and Morales M. (2002) Neoformation of Ni phyllosilicate upon Ni uptake on montmorillonite: A kinetics study by powder and polarized extended x-ray absorption fine structure spectroscopy. *Geochim. Cosmochim. Acta* **66,** 2335–2347.

Dähn R., Scheidegger A. M., Manceau A., Schlegel M. L., Baeyens B., Bradburry M. H., and Chateigner D. (2003) Structural evidence for the sorption of Ni(II) atoms on the edges of montmorillonite clay minerals: A polarized x-ray absorption fine structure study. *Geochim. Cosmochim. Acta* **67,** 1–15.

Elzinga E. and Sparks D. L. (2001) Reaction condition effects on nickel sorption mechanisms in illite-water suspensions. *Soil Sci. Soc. Am. J.* **65,** 94–101.

Furrer G., Zysset M., and Schindler P. W. (1993) Weathering kinetics of montmorillonite: Investigations in batch and mixed-flow reactors. In *Geochemistry of Clay-Pore Fluid Interactions* (eds. Manning D. A. C., Hall, and P. L. Hughes) C. R., Vol. 13 , pp 243–262. Chapman & Hall.

Furrer G., Lothenbach B., Schärli H., and Ludwig C. (1994) Interaction between polynuclear aluminum compounds and heavy metal ions. *J. Eco. Chem.* **3,** 157–162.

Furrer G., Scheidegger A., Plötze M., Kahr G., Studer B., Lothenbach B., and Schulin R. (2001) Specific immobilization of heavy metals in soil using modified montmorillonite *Mitt. Dtsch. Bodenkundl. Ges.* 96:181–182.

Furrer G., Phillips B., Ulrich K. U., Pöthig R., and Casey W. (2002) The origin of aluminum flocs in polluted streams. *Sci.* **297,** 2245–2247.

Greaves C. and Thomas M. A. (1986) Refinement of the structure of deuterated Nickel-hydroxide, $Ni(OD)_2$, by powder neutron-diffraction and evidence for structural disorder in samples with high surface area. *Acta Cryst. B* **42,** 51–55.

Güven N. (1988) Smectites. *Rev. Mineral.* **19,** 497–559.

Harsh J. B. and Donner H. B. (1984) Specific sorption of copper on an hydroxyl-aluminum-montmorillonite complex. *Soil Sci. Soc. Am. J.* **48,** 1034–1039.

Hummel W. and Curti E. (2003) Nickel aqueous speciation and solubility at ambient conditions: A thermodynamic elegy. *Monatsh. Chem.* **134,** 941–973.

Lothenbach B., Furrer G., and Schulin R. (1997) Immobilization of heavy metals by polynuclear aluminium and montmorillonite compounds *Environ. Sci. Technol.* **31,** 1452–1462.

Lothenbach B., Furrer G., Schärli H., and Schulin R. (1999) Immobilization of zinc and cadmium by montmorillonite compounds: Effects of aging and subsequent acidification. *Environ. Sci. Technol.* **33,** 2945–2952.

Manceau A. and Schlegel M. L. (2001) Texture effect on polarized EXAFS amplitude. *Phys. Chem. Minerals* **28,** 52–56.

Manceau A., Llorca S., and Calas G. (1987) Chrystal chemistry of cobalt and nickel in lithiophorite and asbolane from New Caledonia. *Geochim. Cosmochim. Acta* **51,** 105–113.

Manceau A., Chateigner D., and Gates W. P. (1998) Polarized EXAFS distance-valence least-squares modelling (DVLS) and quantitative texture analysis approaches to the structural refinement of Garfield nontronite *Phys. Chem. Minerals* **25,** 347–365.

Manceau A., Schlegel M. L., Musso M., Sole V. A., Gauthier C., Petit P. E., and Trolard F. (2000) Crystal chemistry of trace elements in natural and synthetic goethite. *Geochim. Cosmochim. Acta* **64,** 3643–3661.

Manceau, A., Marcus, M. A., Tamura, N. (2002) Quantitative speciation of heavy metals in soils and sediments by synchrotron x-ray techniques. In *Applications of Synchrotron Radiation in Low-Temperature Geochemistry and Environmental Science* (eds. N. C. Sturchio, P. Fenter, S. R. Sutton and M. L. Rivers), Reviews in Mineralogy. Mineralogical Society of America, Washington, DC.

McBride M. B (1994) *Environmental Chemistry of Soils*. Oxford University Press, New York.

Ressler T. (1998) WinXAS: A program for x-ray absorption spectroscopy data analysis under MS-Windows. *J. Synchr. Rad.* **186,** 118–128.

Roberts D. R., Ford R. G., and Sparks D. L. (2003) Kinetics and mechanisms of Zn complexation on metal oxides using EXAFS spectroscopy. *J. Colloid Interf. Sci.* **263,** 364–376.

Saalfeld H., Wedde M. (1974) Refinement of crystal-structure of gibbsite, $Al(OH)_3$. *Z. Kristallogr.* **139,** 129–135.

Scheidegger A. M., Strawn D. G., Lamble G. M., and Sparks D. L. (1998) The kinetics of mixed Ni-Al hydroxide formation on clay and aluminum oxide minerals: A time-resolved XAFS study. *Geochim. Cosmochim. Acta* **62,** 2233–2245.

Schlegel M. L., Manceau A., Charlet L., Chateigner D., and Hazemann J. L. (2001a) Sorption of metal ions on clay minerals. 3. Nucleation and epitaxial growth of Zn phyllosilicate on the edges of hectorite. *Geochim. Cosmochim. Acta* **65,** 4155–4170.

Schlegel M. L., Manceau A., Charlet L., and Hazemann J. L. (2001b) Adsorption mechanisms of Zn on hectorite as a function of time, pH and ionic strength. *Am. J. Sci.* **301,** 798–830.

Scheinost A. C., Kretschmar R., Pfister S., and Roberts D. R. (2002) Combining selective sequential extractions, x-ray absorption spectroscopy and principal component analysis for quantitative zinc speciation in soil. *Environ. Sci. Technol.* **36,** 5021–5028.

Sparks, D. L. (2003) Environmental Soil Chemistry. Academic Press, London.

Yamaguchi N. U., Scheinost A. C., and Sparks D. L. (2002) Influence of gibbsite surface area and citrate on Ni sorption mechanisms at pH 7.5. *Clays Clay Mineral.* **50,** 784–790.